Analysis of enhanced stimulated Brillouin scattering in silicon slot waveguides

Raphaël Van Laer,[1,2,*] Bart Kuyken,[1,2] Dries Van Thourhout,[1,2] and Roel Baets[1,2]

[1]Photonics Research Group, Ghent University–imec, Belgium

[2]Center for Nano- and Biophotonics, Ghent University, Belgium

*Corresponding author: raphael.vanlaer@intec.ugent.be

Stimulated Brillouin scattering has attracted renewed interest with the promise of highly tailorable integration into the silicon photonics platform. However, significant Brillouin amplification in silicon waveguides has yet to be shown. In an effort to engineer a structure with large photon–phonon coupling, we analyzed both forward and backward Brillouin scattering in high-index-contrast silicon slot waveguides. The calculations predict that gradient forces enhance the Brillouin gain in narrow slots. We estimate a currently feasible gain of about 10^5 W^{-1} m^{-1} in horizontal slot waveguides, which is an order of magnitude larger than in a stand-alone silicon wire. Such efficient coupling could enable a host of Brillouin technologies on a mass-producible silicon chip.   © 2014 Optical Society of America

Stimulated Brillouin scattering (SBS) is a nonlinear process that couples optical to mechanical waves [1,2]. It is a powerful means to control light, with applications ranging from lasing [3], comb generation [4–6], and isolation [7] to RF-waveform synthesis [8], slow/stored light [9,10], and reconfigurable filtering [11]. With this in mind, SBS has been explored in a wide variety of systems, such as conventional and photonic crystal fibers [12–16], silica microspheres [17,18] and wedge-disks [19], calcium fluoride resonators [20], and chalcogenide rib waveguides [21,22]. Therefore the prospect of strong SBS in small-core silicon wires is tantalizing.

Such wires are known for their large Kerr and Raman nonlinearity [23]. However, Brillouin scattering has so far lagged behind in silicon. The culprit is the silica substrate on which the silicon wires are typically made. It severely decreases both the wires' mechanical flexibility and the phonons' lifetime. Unlike in chalcogenide rib waveguides [21,24], elastic waves in silicon cannot be guided by internal reflection because sound is faster in silicon than in silica.

A theoretical model by Wang *et al.* [25,26] recently predicted that the efficiency of SBS would increase dramatically by removing the substrate. Then the elastic waves are confined to the core because of the large acoustic mismatch between air and silicon, although there is still no internal reflection. The model included not just electrostriction but also radiation pressure, which was traditionally neglected as a driver of Brillouin scattering. Thus electrostriction and radiation pressure interfere in nanoscale waveguides, connecting the fields of Brillouin scattering and optomechanics [27,28]. The validity of the new SBS model has been confirmed by recent observations of SBS in a hybrid silicon nitride-silicon waveguide [29], although the enhancement of SBS in silicon-only photonic wires [25,26] remains unverified.

In this Letter, we take the study of Brillouin scattering to silicon slot waveguides to exploit their strong optical mode confinement [30,31] and large gradient forces [32]. We perform full-vectorial coupled optical and mechanical simulations of the Brillouin gain coefficient using the finite-element solver COMSOL.

We consider vertical [Figs. 1(a) and 1(b)] and horizontal [Figs. 1(c) and 1(d)] slot waveguides suspended in air. Both waveguides strongly confine light, creating large radiation pressure close to the slot. This gives rise to the possibility of (1) improving the photon–phonon coupling, (2) testing SBS theory in a regime dominated by gradient forces, and (3) exciting new types of phonons.

A particular mechanical mode with displacement $\mathbf{u}$, wavevector K, stiffness per unit length k_{eff}, and quality factor Q has a peak SBS gain G of $\omega Q|\langle\mathbf{f},\mathbf{u}\rangle|^2/(2k_{\text{eff}})$, with ω the optical frequency, $\mathbf{f} = \mathbf{f}_{\text{rp}} + \mathbf{f}_{\text{es}}$ the power-normalized force distribution, and $\langle\mathbf{f},\mathbf{u}\rangle = \int \mathbf{f}^* \cdot \mathbf{u}dA$ the photon–phonon overlap [25,26]. The radiation pressure $\mathbf{f}_{\text{rp}}$ is located on the waveguide boundaries [Fig. 2(a)], while the electrostrictive force $\mathbf{f}_{\text{es}}$ has both
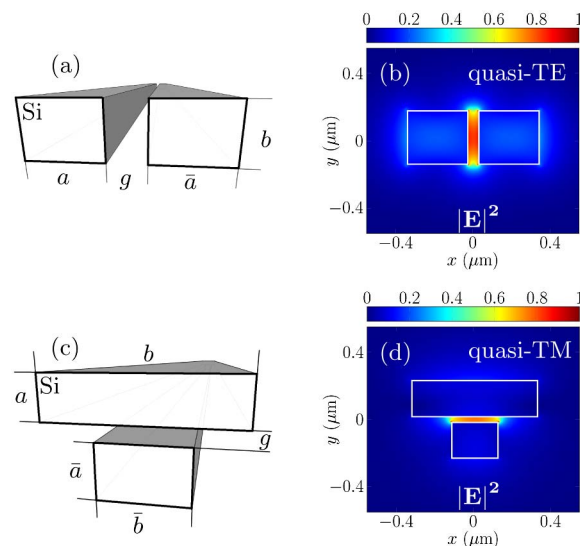

Fig. 1.   (a) Vertical and (c) horizontal silicon slot waveguides suspended in air, with the corresponding optical mode (b) and (d).
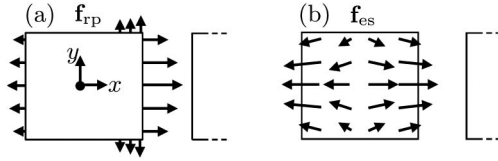
Fig. 2. Typical optical force profile on left beam of vertical slot waveguide: (a) radiation pressure and (b) electrostrictive body force. The radiation pressure is large close to the slot.

a body [Fig. 2(b)] and a boundary (not shown) component. The boundary component of $\mathbf{f}_{es}$ is an order of magnitude smaller than $\mathbf{f}_{rp}$. Furthermore, we define G_{rp} and G_{es} as the SBS gain when only $\mathbf{f}_{rp}$ or $\mathbf{f}_{es}$ is present. The total gain G is determined by interference between $\mathbf{f}_{rp}$ and $\mathbf{f}_{es}$. Additionally, the pump and Stokes wave co-(counter-) propagate in forward (backward) SBS. Phase-matching then requires that $K \approx 0$ ($K \approx 2\beta$), with β the pump wavevector. Finally, we work at $\lambda = 1.55$ μm, use a flat Q of 10^3 as in [25,26] and we launch the pump and Stokes wave into the same optical mode [Figs. 1(b)–1(d)].

If the two beams have identical width and height [Fig. 3(a)], their mechanical resonances can be addressed simultaneously. Then the gain is $4G$, since the total overlap $\langle \mathbf{f}, \mathbf{u} \rangle$ is twice the overlap over a single beam. However, these dimensions cannot differ by more than a fraction $1/Q$ to align the resonances within one mechanical linewidth. This is technologically challenging with a Q of about 10^3. So we assume just one beam of dimensions (a, b) contributes to SBS [Fig. 3(b)], even though the unexcited beam may also be suspended. Moreover, in wide slots the optical mode evolves into the symmetric supermode of two weakly coupled silicon wires. So $4G \to \tilde{G}$ as $g \to \infty$, with $\tilde{G}$ the peak gain associated with a phonon in a stand-alone wire [Fig. 3(c)]. In other words, the slot waveguide [Fig. 3(b)] has to overcome a factor 4 to reach the $G/\tilde{G} > 1$ gain enhancement regime.

Figures 4(a)–4(c) show the forward and backward SBS spectrum for a vertical slot waveguide with dimensions $(a, b, \bar{a}, g) = (315 \text{ nm}, 0.9a, a, 50 \text{ nm})$, including only the three modes with largest gain.

In the forward case [Fig. 4(a)], the mechanical modes are identical to those of a stand-alone wire. The maximum gain among all modes is $4.2 \times 10^3 \text{ W}^{-1} \text{m}^{-1}$. This is smaller than $\tilde{G}/4 = 4.3 \times 10^3 \text{ W}^{-1} \text{m}^{-1}$ [26], despite the increase in radiation pressure close to the slot. The cause is a decrease in the pressure on the far side from the slot [Fig. 2(a)]. This decrease cancels out the enhanced forces close to the slot, even in slots as narrow as 50 nm. This also explains why G does not change significantly for $g > 50$ nm [Fig. 4(b)]. Hence, smaller gaps are necessary to boost G substantially. Indeed, for the most promising mode we numerically find that $G \propto 1/g$
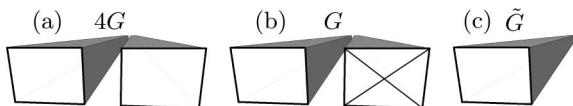

Fig. 3. (a) Slot with two mechanically excited beams, (b) slot with just one excited beam, and (c) a stand-alone wire. We work in scenario (b).
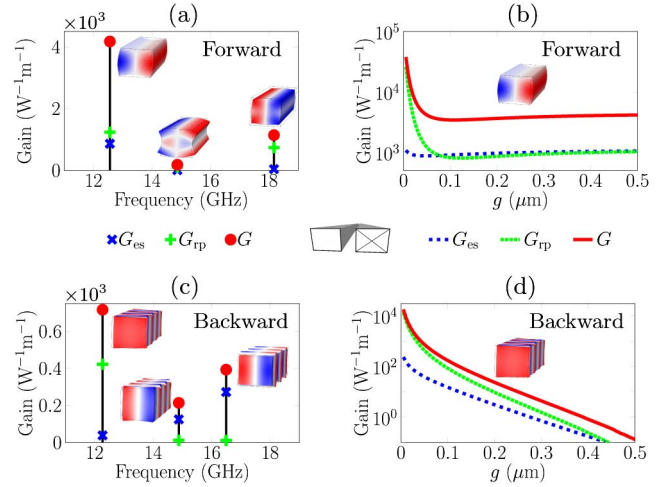

Fig. 4. (a)–(c) Brillouin spectrum of a vertical slot waveguide and (b)–(d) the gain of the most promising mode increases rapidly in narrow slots. The color of the modes indicates the sign of u_x (red: +, blue: −).

as g falls below 50 nm [Fig. 4(b)]. Eventually G approaches a maximum of $\approx 1.1 \times 10^5 \text{ W}^{-1} \text{m}^{-1}$ as $g \to 0$.

In the backward case, the mechanical modes are different from those of a stand-alone wire since the phonon wavevector $K \approx 2\beta$ depends on the effective index n_p of the optical mode. From the point of view of a single beam, horizontal symmetry is broken by the slot waveguide. So modes that were previously forbidden by symmetry can have nonzero gain in the slot waveguide. Such a previously forbidden phonon has the largest backward SBS gain in the slot waveguide [Fig. 4(c)]. For $g = 50$ nm, this phonon has a gain of $7.2 \times 10^2 \text{ W}^{-1} \text{m}^{-1}$. The optical forces are symmetric again in wide slots. Then this mode is forbidden, which means that $G \to 0$ as $g \to \infty$ [Fig. 4(d)]. Going from wide to narrow slots, G first increases exponentially; then its growth accelerates like $G \propto 1/g^{1.6}$ and ultimately converges to a maximum of $\approx 4.5 \times 10^4 \text{ W}^{-1} \text{m}^{-1}$ as $g \to 0$.

In general, gradient forces dominate the SBS gain in narrow slots [Fig. 4(b)–4(d)]. The slot enhances these forces despite the reduced dispersion in such waveguides. As $g \to 0$, the group and effective indices n_g and n_p approach those of a single wire of width $a + \bar{a}$. Thus the waveguide dispersion decreases [Fig. 5(a)], contrary to the prediction that very dispersive waveguides are optimal for large gradient forces [33]. Writing the power-normalized gradient force density as $\mathbf{p}\delta(\mathbf{r} - \mathbf{r}_{\partial wg})$, it was shown that $c \int \mathbf{p} \cdot \mathbf{r} dl = n_g - n_p$ from the scale-invariance of Maxwell's equations [33]. For a stand-alone wire the integral becomes $\int \mathbf{p} \cdot \mathbf{r} dl = A_{wg}(\bar{p}_x + \bar{p}_y)$ with $A_{wg} = ab$ and $\bar{p}$ the magnitude of the spatially averaged radiation pressure. However, this no longer holds for a slot waveguide. Then the integral yields $\int \mathbf{p} \cdot \mathbf{r} dl = A_g(\bar{p}_{x,L} - \bar{p}_{x,R}) + 2A_{wg}(\bar{p}_{x,L} + \bar{p}_y)$, with $\bar{p}_{x,L/R}$ the pressure on the left/right boundary, $A_g = gb$ and $a = \bar{a}$. Since $A_g \to 0$ as $g \to 0$, $\bar{p}_{x,R}$ and thus $\bar{p}_x + \bar{p}_y$ can increase drastically in narrow slots [Fig. 5(a)].

Next, we investigate the effect of $\bar{a}$ [Fig. 5(b)–5(d)]. As $\bar{a} \to 0$, there is no slot-enhancement. Then $G \to \tilde{G}$, regardless of all other parameters. Furthermore, the optical mode increasingly retreats into the widest beam. This
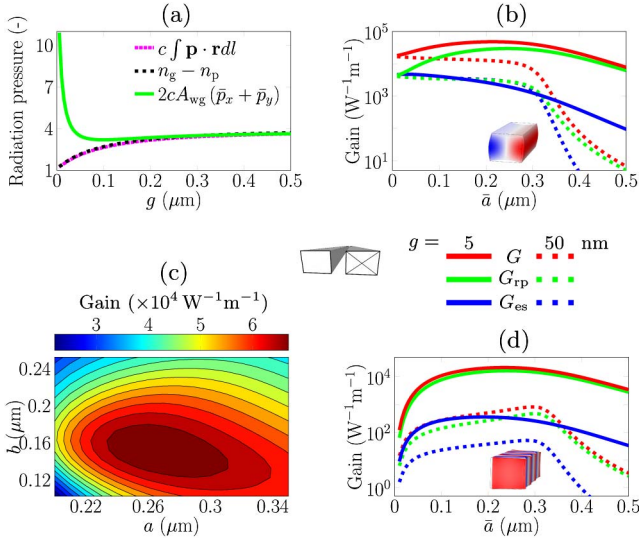
Fig. 5.   (a) Gradient forces can be large despite low dispersion; (b)–(d) narrow slots perform better than a stand-alone wire for a range of $\bar{a}$-values; and (c) G has a clear optimum in the (a, b)-plane for the same mode as in (b) with $g = 5$ nm.

implies $G \to 0$ when $\bar{a} \to \infty$, although this effect is more pronounced in wider slots.

In the forward case [Fig. 5(b)], $\bar{a}$ affects only the force distribution. The gain $G(\bar{a})$ has a maximum in narrow slots but decreases monotonically otherwise. This confirms that small gaps are required for substantial gain enhancement in vertical slot waveguides.

In the backward case [Fig. 5(d)], $G(\bar{a})$ always has a maximum because this phonon is forbidden in a stand-alone wire. However, the maximum increases by a factor 26 when the slot is narrowed from 50 to 5 nm. The gain is dominated by gradient forces regardless of $(\bar{a}, g)$.

Last, we scan (a, b) with $\bar{a} = a$ and g fixed at 5 nm. These parameters influence both the optical and mechanical mode. The (a, b)-optimum depends heavily on the slot size and on the mechanical mode. Nonetheless, Fig. 5(c) shows that there actually exists such an optimum. We find a maximum gain of 7.0×10^4 W^{-1} m^{-1} for $(a, b) = (260, 150)$ nm.

The horizontal slot [Fig. 1(c) and 1(d)] has the potential advantage of (1) the extra degree of freedom $\bar{b}$ and (2) smaller gaps. In such a slot, g is not limited by the resolution of lithography techniques. As a result, SBS enhancement may be within reach of current technology. As long as $\bar{b} = b$, the horizontal slot waveguide is but a rotated version of the vertical one. Therefore we immediately explore the case $\bar{b} \neq b$. We calculate the forward and backward Brillouin spectrum for a horizontal slot waveguide with dimensions $(a, b, \bar{a}, \bar{b}, g) = (160, 620, a, 240, 5)$ nm.

In the forward case [Fig. 6(a)], the fundamental flexural mode couples most efficiently. This mode has negligible SBS gain in a stand-alone wire because of cancellations in the photon–phonon overlap. Indeed, the u_y component has two nodes, while the y component of the gradient force does not change sign. Owing to $b > \bar{b}$, the cancellations can be avoided by confining the optical mode between the nodes of u_y.

In the backward case [Fig. 6(c)], there are two modes with enhanced coupling. The first mode has a nearly

uniform u_y component. It is a rotated version of the mode we previously studied in Figs. 4(d) and 5(d). The second mode is the fundamental flexural mode, but at the operating point $K \approx 2\beta$ in its dispersion diagram.

The gain increases by four orders of magnitude when g drops from 250 to 5 nm [Fig. 6(b)]. This radical enhancement is superexponential in g for gaps below 50 nm. The forward (backward) gain approaches $\approx 1.3 \times 10^6$ W^{-1} m^{-1} (1.5×10^5 W^{-1} m^{-1}) as $g \to 0$. At $g = 70$ nm, an optical mode anti-crossing causes a dip in the SBS gain. However, $G(g)$ quickly recovers its original path as g leaves the anti-cross region. We only show the total gain G because G_{es} is at least a factor 10^5 (10^2) smaller than G_{rp} across the entire sweep range in the forward (backward) case. Thus SBS by these modes is driven by gradient forces only, with a vanishing electrostrictive contribution.

Finally, we sweep $\bar{b}$ [Fig. 6(d)]. In the forward case, k_{eff} and $\mathbf{u}$ do not depend on $\bar{b}$. Then we explore purely the effect of the gradient force density $\mathbf{f}_{rp}(\bar{b})$ on the photon–phonon overlap $\langle \mathbf{f}_{rp}(\bar{b}), \mathbf{u} \rangle$. The coupling is optimal for $\bar{b} = 240$ nm. For smaller $\bar{b}$, G decreases because the slot-enhancement occurs only in a small region. For larger $\bar{b}$, G decreases because the optical mode is no longer confined between the nodes of u_y. In the backward case, the operating point $K \approx 2\beta$ changes as n_p depends on $\bar{b}$. This propagating phonon is less sensitive to $\bar{b}$ because of its nearly uniform u_y component.

To conclude, we found that strong gradient forces improve the efficiency of Brillouin scattering in narrow silicon slot waveguides. However, appreciable enhancement compared to a stand-alone wire is currently only accessible in horizontal slots. In such slots, we expect very efficient SBS because (1) small gaps should be technologically feasible and (2) the fundamental mechanical flexural mode can be excited. The suspension of long silicon beams remains the most important hurdle toward testing these predictions. A practical device may consist of a disconnected series of such waveguides as in [29]. With a coupling of 10^5 W^{-1} m^{-1}, the simulations predict
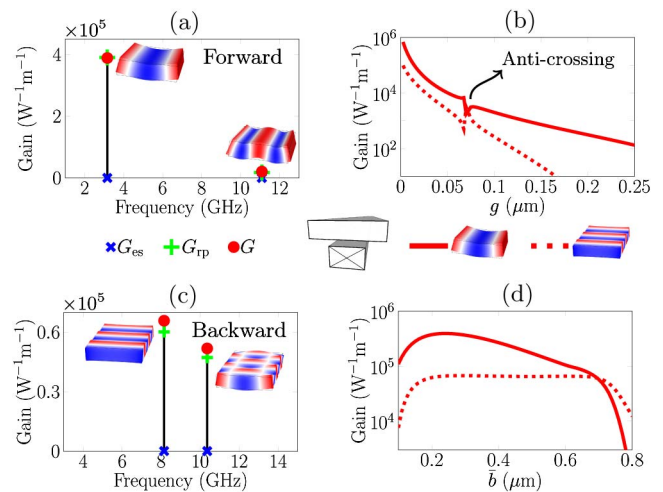

Fig. 6.   (a)–(c) Both forward and backward SBS is very efficient in narrow horizontal slots and (d) the flexural mode is sensitive to $\bar{b}$. The color of the modes indicates the sign of u_y (red: +, blue: −).

that 20 dB gain is feasible with 50 mW on-chip pump power over 1 mm propagation length.

Supplementary information: We use isotropic elasticity coefficients $(c_{11}, c_{12}, c_{44}) = (217, 85, 66)$ GPa for easy comparison with [25,26]. Silicon is mechanically anisotropic, so in a more accurate calculation the coefficients $(c_{11}, c_{12}, c_{44}) = (166, 64, 80)$ GPa should be used for a guide along a $\langle 100 \rangle$ crystal axis [34]. Further, we use the photoelastic coefficients $(p_{11}, p_{12}, p_{44}) = (-0.094, 0.017, -0.051)$ [35], which is also valid in case the guide is aligned along a $\langle 100 \rangle$ axis. We perform our calculations using the weak-form [36] COMSOL module with the MATLAB Livelink.

References

1. R. Chiao, C. Townes, and B. Stoicheff, Phys. Rev. Lett. **12**, 592 (1964).
2. Y. Shen and N. Bloembergen, Phys. Rev. **290**, 1787 (1965).
3. L. Stokes, M. Chodorow, and H. Shaw, Opt. Lett. **7**, 509 (1982).
4. D. Braje, L. Hollberg, and S. Diddams, Phys. Rev. Lett. **102**, 1 (2009).
5. M. Kang, A. Nazarkin, A. Brenn, and P. Russell, Nat. Phys. **5**, 276 (2009).
6. A. Savchenkov, A. Matsko, V. Ilchenko, D. Seidel, and L. Maleki, Opt. Lett. **36**, 3338 (2011).
7. M. Kang, A. Butsch, and P. Russell, Nat. Photonics **5**, 549 (2011).
8. J. Li, H. Lee, and K. Vahala, Nat. Commun. **4**, 1 (2013).
9. Y. Okawachi, M. Bigelow, J. Sharping, Z. Zhu, A. Schweinsberg, D. Gauthier, R. Boyd, and A. Gaeta, Phys. Rev. Lett. **153902**, 1 (2005).
10. Z. Zhu, D. Gauthier, and R. Boyd, Science **318**, 1748 (2007).
11. A. Zadok, A. Eyal, and M. Tur, J. Lightw. Technol. **25**, 2168 (2007).
12. E. Ippen and R. Stolen, Appl. Phys. Lett. **21**, 539 (1972).
13. R. Shelby, M. Levenson, and P. Bayer, Phys. Rev. Lett. **54**, 939 (1985).
14. A. Kobyakov, M. Sauer, and D. Chowdhury, Adv. Opt. Photon. **2**, 1 (2010).
15. J. Wang, Y. Zhu, R. Zhang, and D. Gauthier, Opt. Express **19**, 5339 (2011).
16. J. Beugnot, T. Sylvestre, and H. Maillotte, Opt. Lett. **32**, 17 (2007).
17. M. Tomes and T. Carmon, Phys. Rev. Lett. **102**, 113601 (2009).
18. G. Bahl, J. Zehnpfennig, M. Tomes, and T. Carmon, Nat. Commun. **2**, 403 (2011).
19. J. Li, H. Lee, T. Chen, and K. Vahala, Opt. Express **20**, 369 (2012).
20. I. Grudinin, A. Matsko, and L. Maleki, Phys. Rev. Lett. **102**, 043902 (2009).
21. R. Pant, C. Poulton, D. Choi, H. Mcfarlane, S. Hile, E. Li, L. Thevenaz, B. Luther-Davies, S. Madden, and B. Eggleton, Opt. Express **19**, 8285 (2011).
22. B. Eggleton, C. Poulton, and R. Pant, Adv. Opt. Photonics **5**, 536 (2013).
23. Q. Lin, O. Painter, and G. Agrawal, Opt. Express **15**, 416 (2007).
24. C. Poulton, R. Pant, and B. Eggleton, J. Opt. Soc. Am. B **30**, 1 (2013).
25. P. Rakich, C. Reinke, R. Camacho, P. Davids, and Z. Wang, Phys. Rev. X **2**, 1 (2012).
26. W. Qiu, P. Rakich, H. Shin, H. Dong, M. Soljačić, and Z. Wang, Opt. Express **21**, 31402 (2013).
27. T. Kippenberg and K. Vahala, Opt. Express **15**, 17172 (2007).
28. D. Van Thourhout and J. Roels, Nat. Photonics **4**, 211 (2010).
29. H. Shin, W. Qiu, R. Jarecki, J. Cox, R. Olsson, A. Starbuck, Z. Wang, and P. Rakich, Nat. Commun. **4**, 1944 (2013).
30. V. Almeida, Q. Xu, C. Barrios, and M. Lipson, Opt. Lett. **29**, 1209 (2004).
31. R. Sun, P. Dong, N. Feng, C. Hong, J. Michel, M. Lipson, and L. Kimerling, Opt. Express **15**, 17967 (2007).
32. M. Li, W. Pernice, and H. Tang, Appl. Phys. Lett. **97**, 183110 (2010).
33. P. Rakich, Z. Wang, and P. Davids, Opt. Lett. **36**, 217 (2011).
34. M. Hopcroft, W. Nix, and T. Kenny, J. Microelectromech. Syst. **19**, 229 (2010).
35. D. Biegelsen, Phys. Rev. Lett. D **32**, 1196 (1974).
36. S. Dasgupta and F. Poletti, J. Lightw. Technol. **29**, 22 (2011).